Exp Fluids (2013) 54:1492
DOI 10.1007/s00348-013-1492-8

RESEARCH ARTICLE

# Flow control for aero-optics application

**B. Vukasinovic · A. Glezer · S. Gordeyev · E. Jumper · W. W. Bower**

Received: 20 April 2012 / Revised: 11 February 2013 / Accepted: 22 February 2013 / Published online: 15 March 2013


**Abstract** The mitigation of aero-optical aberrations in the wake of a surface-mounted turret comprised of a hemisphere mounted on a matching cylindrical support is investigated in wind tunnel experiments. The effects of hybrid (passive/active) flow control on the aero-optical and aerodynamic characteristics of the flow over a conformal optical aperture embedded in the hemispherical cap are investigated at $M = 0.3$ and $Re_D = 4.46 \times 10^6$. Direct optical diagnostics of 2D wavefronts over the aperture is performed using a high-speed Shack-Hartmann wavefront sensor for a range of aperture orientations on and off the streamwise center plane. Aerodynamic flow diagnostics includes arrays of static and dynamic pressure ports on the turret and the ground plane that help characterize flow separation and the wake topology. The global flow is passively controlled by a forward-facing partition plate that increases the flow receptivity to and the effectiveness of arrays of high-frequency fluidic oscillating jets that are placed upstream of the aperture. It is shown that the hybrid flow control yields significant improvements in the aero-optical characteristics of the flow over the aperture that exceeds the individual effects of passive and active control.

This article is a part of the collection Topics in Flow Control. Guest Editors J. P. Bonnet and L. Cattafesta.

B. Vukasinovic (✉) · A. Glezer
Woodruff School of Mechanical Engineering, Georgia Institute of Technology, Atlanta, GA 30332-0405, USA
e-mail: bojan.vukasinovic@me.gatech.edu

S. Gordeyev · E. Jumper
Department of Aerospace and Mechanical Engineering, University of Notre Dame, Notre Dame, IN 46556, USA

W. W. Bower
The Boeing Company, MC S306-430, P.O. Box 516, Saint Louis, MO 63166, USA

**List of symbols**

| | |
|---|---|
| $A_j$ | Exit area of the actuator orifice |
| $A_o$ | Frontal turret area |
| $C_p$ | Pressure coefficient |
| $C_\mu$ | Mass flow rate coefficient |
| $D$ | Turret diameter |
| $f$ | Frequency |
| $M$ | Freestream Mach number |
| OPD | Optical path difference |
| $OPD_{rms}$ | Spatial root-mean-square of OPD |
| $R$ | Turret radius |
| $R_A$ | Optical aperture radius |
| $Re_D$ | Reynolds number |
| $St_D$ | Strouhal number |
| $U_0$ | Freestream velocity |
| $U_j$ | Average jet velocity |
| $H$ | Height of turret base |
| $\alpha$ | Elevation angle of optical aperture |
| $\beta$ | Azimuthal angle of optical aperture |
| $\delta$ | Boundary layer thickness |
| $\gamma$ | Local azimuth angle of pressure ports |
| $\rho$ | Air density |
| $\rho_{SL}$ | Sea-level air density |

## 1 Introduction

When an optical wavefront passes through an inhomogeneous density field, its wavefront becomes distorted or aberrated due to a linear dependence between the density and the index-of-refraction; these distortions are referred to

as an aero-optical problem (Gilbert and Otten 1982; Wang et al. 2012). The wavefront distortions, combined with optical aberrations caused by the wavefront propagation through the atmosphere, known as an atmospheric propagation problem (Tatarskii and Zavorotnyi 1985), ultimately degrade the light intensity from the otherwise diffraction-limited intensity at the destination. These aero-optical aberrations typically have high spatial and temporal bandwidths which are well outside the current control capabilities of traditional adaptive-optics methods (Jumper and Fitzgerald 2001).

Turrets on airborne platforms are bluff-body protrusions that typically consist of a hemispherical cap supported by a matching cylindrical base. They provide convenient housing for pointing and tracking laser beams from airborne platforms, either for direct energy or for high-speed and secure free-space communication purposes. An optical aperture is therefore built into the turret cap and can be either flat or conformal. On the other hand, turrets create turbulent separated flows and wakes that can distort an otherwise planar laser beam even at relatively low subsonic speeds (Gordeyev and Jumper 2010). Consequently, this leads to the laser beam's unsteady defocus and jitter (Gilbert and Otten 1982) and can even break the beam into separate spots. Separated shear layers, such as those in the near wakes of bluff bodies, are particularly destructive because of the presence of large coherent vortical structures that are known to be a major source of optical wavefront distortion, since they induce strong pressure and therefore density gradients (Fitzgerald and Jumper 2004). Moreover, the three-dimensional flow separation on turret-like bluff bodies is accompanied by the formation of 3D vortical eddies that evolve into two counter-rotating streamwise vortices off the aft surface of the turret (e.g., review article by Gordeyev and Jumper 2010) and are often referred to as the 'horn' vortices. The presence of these vortices can lead to further significant degradation in optical transmission through the near wake of the turret. Left untreated, these vortical-related optical aberrations can limit an airborne transmitting system to a forward-looking quadrant only. In order to extend viewing angles to at least a portion of an aft-looking quadrant, a region of the optically traversed flow can be extended by delaying separation of the flow and/or by disrupting formation of the large-scale shear-layer vortices.

Control of the flow over a turret that houses a laser-based optical system must satisfy more stringent requirements than "traditional" separation control over external aerodynamic surfaces. Whereas the effectiveness of flow control on aerodynamic surfaces can be typically evaluated in terms of its effect on the time-averaged aerodynamic forces and moments, the intent of aero-optical flow control is to enhance transmission of a laser beam through regions of separated turbulent flow dominated by compact and fast-moving vortical structures. Thus, both spatial and temporal flow dynamics along the beam path need to be altered or mitigated, rather than just static (mean) effects on the flow.

The intent of the work presented in this paper is to demonstrate the effectiveness of combined active and passive flow control of the unsteady aerodynamic environment around a conformal-aperture turret for achieving significant improvement in minimizing laser wavefront degradation over a wide range of viewing angles in the back-looking quadrant.

Most of the previous work on flow control of separated flows over bluff-body protrusions has been directly motivated by the aero-optical problems involving an airborne turret having either flat or conformal optical aperture. A number of studies were conducted in low-speed, incompressible flows ($M < 0.15$), where potential aero-optics benefits were typically inferred from the flow control effects on suppression of either velocity or surface pressure fluctuations. One of the earliest attempts of low-speed flow control aimed at improving the aero-optical environment around turret was reported by Schonberger et al. (1982), where the proposed control approach involved a combination of a long aft fairing (passive) and dual suction (active) components at the support surface, integrated into the long fairing. Vukasinovic and Glezer (2007) demonstrated the effectiveness of fluidic, direct high-frequency control in turbulence suppression behind a bluff-body turret at $Re_D = 8 \times 10^5$. Woszidlo et al. (2009) investigated the effects of passive generation of streamwise vortices in the oncoming wall boundary layer and active steady suction at the trailing-edge base on separation of the low-speed flow over the spherical protuberances at Reynolds numbers up to $3 \times 10^5$. The former delayed separation off the surface, while the latter was able to remove necklace vortices around the protuberance and thereby eliminate one source of vorticity and turbulence intensity in the wake. The effectiveness of direct, small-scale control ($St_D > 10$) of the separated flow over a hemispherical protuberance with a thin upstream boundary layer was demonstrated (Vukasinovic et al. 2009) at $Re_D = 4{-}7 \times 10^5$. They showed that the presence of flow control can substantially reduce the extent of the recirculating domain downstream of the hemisphere with significant reduction in turbulent kinetic energy. Wallace et al. (2010) explored both open- and closed-loop control schemes on a flat-aperture turret in static and dynamic pitching attitudes ($Re_D = 4.5 \times 10^5$). The control was effected by the variable duty cycle suction slots distributed around the aperture, and it was shown that both open- and closed-loop control schemes significantly suppress the measured velocity fluctuations within the wake, while the closed-loop control appeared to be more efficient. Another active control tool that was explored at

low speeds ($Re_D = 4 \times 10^4$) was plasma-induced actuation (Catrakis et al. 2011), where the control authority was demonstrated in terms of the delay of flow separation.

A subset of the flow control studies was conducted in the compressible flow regime (predominantly $M \geq 0.3$), having an aerodynamic measure of effectiveness, i.e., without a direct aero-optical characterization of the flow. An early numerical work by Purohit et al. (1983) predicted significant favorable alteration of the turret wake structure when investigating low levels of distributed suction through the porous hemispherical shell. Numerical work by Morgan and Visbal (2009) further emphasized that distributed porous suction over forward turret surface significantly delayed separation off the turret surface at $M = 0.4$ and consequently reduced the wake extent and its turbulent intensity. Patil and Ng (2010) proposed a suction pattern on the support cylinder and showed the CFD results that indicated a significant delay in the flow separation due to the two control-induced, large-scale streamwise vortices. Andino et al. (2011) presented the open- and closed-loop control results for the flat-aperture turret at fixed orientation, where the control was effected by an array of synthetic jets distributed around the aperture. They showed that the open-loop control reduced the level of surface pressure fluctuations by about 20 %, while the closed-loop control resulted in suppression of about 25 %, and also induced homogeneous scales of surface pressure fluctuations across the aperture. Palaviccini et al. (2011) presented a systematic study of passive pin arrays distributed upstream of separation of a turret with a flat aperture, at speeds up to $M = 0.26$. Their dynamic pressure measurements over the aperture and complementary surface flow visualizations revealed that a significant separation delay and suppression of the wake were associated with an actual increase in the level of aperture surface pressure fluctuations. Contrary to this scenario, the control case that resulted in most suppression of the aperture surface pressure fluctuations actually increased the wake domain.

The aero-optical aberrations in the 3D separated flow have rich contents in both the spatial and temporal domains. Due to inherent measurements complexity, the aero-optics diagnostics often resolves either temporal (e.g., Malley probe) or spatial (e.g., uncorrelated 2D Wavefront sensors) content. Vukasinovic et al. (2010a) measured both aerodynamic and aero-optical effects of synthetic jet active control of the flow over a turret, nominally at $M = 0.3$ and $Re_D = 4.5 \times 10^6$. It was shown that aerodynamic improvements in separation delay and suppression of turbulent energy within the wake resulted in about 30 % suppression in optical aberrations, as measured directly at the conformal aperture center by the Malley probe. Gordeyev et al. (2010) studied the effects of the passive pins distributed upstream from the pseudo 2D "turret" with a flat aperture. The aero-optical characterization included both the Malley probe and the uncorrelated 2D wavefront sensor for different aperture elevation angles. They concluded that a fine balance between the pin-induced shear layer and the turret shear layer in a double non-interacting shear-layer configuration was necessary for consistent 20 % reduction in optical aberrations across the elevation angles. Wallace et al. (2011) reported significant suppression of optical aberrations over a turret flat aperture when the suction control was applied through the slots distributed around the aperture, as measured by the Malley probe. The suppression was directly proportional to the suction duty cycle. They also reported that the level of surface pressure fluctuations over the aperture increases as the optical aberrations decrease in the controlled flows. Vukasinovic et al. (2011) proposed a simultaneous active (synthetic jets) and passive (forward partition plate) control approach, coined as 'hybrid', in an effort to impose both local/shear-layer and global/topology alterations of the flow. The accompanying Malley probe measurements for the varying look-back elevation angles and the fixed azimuth angle of the conformal aperture indicated a favorable control effect along the measured path.

The present investigation builds on the earlier findings of work on active control of the flow over an optical turret by direct small-scale excitation (Vukasinovic and Glezer 2007; Vukasinovic et al. 2010a) and on hybrid (passive/active) flow control (Vukasinovic et al. 2011). A novel element of the present work is the use of dual aero-optics flow diagnostics, where a high-speed 2D wavefront sensor is utilized to acquire simultaneous temporally and spatially resolved measurements of optical aberrations, while a Malley probe is utilized as a secondary diagnostic tool. The experimental setup and diagnostics are described in Sect. 2. The characterization of the base flow is described in Sect. 3, 4 presents the results of active and hybrid control, respectively. Finally, the conclusions are presented in Sect. 5.

## 2 Experimental setup and diagnostics

The present investigation was conducted at the Subsonic Aerodynamic Research Laboratory (SARL) at Wright-Patterson Air Force Base in an open-loop indraft wind tunnel with a 2.13 × 3.05 m octagonal test section that is 4.57 m long. The test section was custom designed for maximal optical access, having 28 windows built into the test section walls, comprising 56 % of the test section surface area. The tunnel has a 14 × 15.2 m inlet, giving a 35:1 contraction ratio. Honeycomb and screens are installed in the inlet before the contraction for turbulence intensity management. The test section Mach number was

kept constant at $M = 0.3$ for all the experimental cases, which corresponds to $Re_D = 4.46 \times 10^6$.

The turret model consists of a $D = 0.61$ m diameter hemispherical cap that is supported on a matching cylinder of $H = 0.19$ m in height (Fig. 1a). The model is equipped with a 0.254 m diameter conformal optical aperture/mirror assembly, which is used for reflection of either the 0.254 m diameter laser beam of the high-speed 2-D wavefront sensor or the 1.5 mm Malley Probe laser beams. The lower section of the cylindrical turret base is stationary, but allows for rotation of the upper model about the turret's zenith plane, thereby positioning the aperture azimuth angle $\beta$. The central hemispherical section between the side trunnions can also be rotated, providing the adjustment of the aperture elevation angle $\alpha$, which is defined as the angular position of the aperture's center, relative to the freestream flow direction. Each combination of the elevation and azimuth angles constitutes turret attitude (Fig. 1a), which is denoted in the remainder of this paper as (elevation, azimuth) in degrees.

Active flow control was effected by arrays of fluidic oscillating (FO) jets, which operation is based on natural internal flow instabilities that convert steady air flow at the inlet to unsteady jets that oscillate in a plane that is defined by the major axis of the actuator's exit aperture ($A_j = 4.5$ mm $\times$ 1.5 mm). Each actuator aperture was oriented such that its long side was approximately perpendicular to the outer flow when the optical aperture is located at $\beta = 180°$ for the center plane tests. When the optical aperture was oriented off the center plane, the actuators configuration was altered so that their orientation relative to the free stream was maintained at $\beta = 136°$. Additional information on the development and characterization of fluidic oscillators can be found in a number of earlier works (e.g., Gregory et al. 2007). The turret fluidic oscillating jets were distributed over four control zones, as shown schematically in Fig. 1b, that could be addressed individually. The Zone 1 is closest to the aperture and it was utilized in all of the control scenarios. The next upstream band of control sources is added for the near-horizontal elevation angles and is also split in two halves, labeled as Zone 2 and 3. Lastly, the most upstream segment is labeled as Zone 4, and it is aimed at the lowest combinations of both elevation and azimuth angles. A total of 180 fluidic oscillator (FO) orifices were distributed across all control zones: Zone 1 consists of three rows of 30 FOs (for a total of 90) arranged upstream and around the optical aperture at angles of 33°, 39°, and 45° from the optical aperture axis. Zones 2 and 3 each contain two rows of 15 FOs (for a total of 30 each), with the rows located at angles of 55°, and 65° from optical aperture axis. Zone 4 consists of 30 FOs, which are positioned in 6 rows. A relative net mass flow addition to the flow is characterized by the mass flow rate coefficient $C_\mu$, which is defined as a total mass flow rate through the active jets divided by the tunnel mass flow rate through the turret frontal cross-sectional area $A_o$, and $C_\mu$ was of the order of $10^{-3}$ for all of the control cases considered. Besides the nominal turret geometry, a modified geometry included a passive flow control component, a partition plate (Fig. 1c). A concept of passive alteration of the global flow topology over a turret by addition of a partition plate was already explored (Vukasinovic et al. 2011), where its effectiveness was demonstrated in passive and hybrid flow control configurations. There are two main reasons for the use of the partition plate as a passive flow control component. It helps suppressing the turret wake by displacing the front stagnation line farther downstream along the hemisphere surface and thereby inducing a thinner boundary layer and delayed separation on the aft surface of the hemisphere. In addition, the plate itself generates a necklace vortex to further assist in diminishing the effects of flow separation along the hemisphere's sides. The present plate's frontal part is formed by an ellipse having major and minor axes of $1.8R$ and $1.5R$, respectively, and whose center is displaced by R/6 upstream from the turret center. The aft segment of the partition plate wraps around turret at radius $1.5R$ through $\beta = 120°$. The downstream edge of the partition plate is deflected downward by 10° for $90° < \beta < 120°$, thereby creating the aft lifting surface.

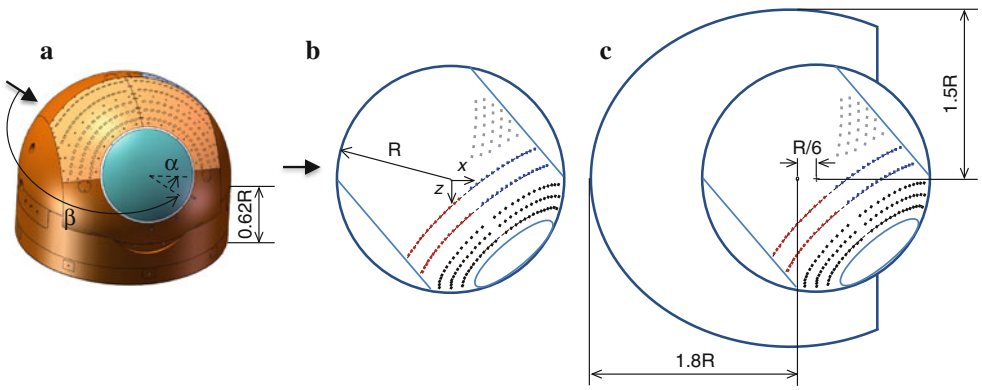


**Fig. 1** A base turret model (**a**) and *top-view* schematics of the flow control approaches in active (**b**) and passive/hybrid (**c**) configurations for the aperture attitude ($\alpha = 30°$, $\beta = 136°$). Fluidic oscillating jet arrays are distributed in Zone: 1 (*black*), 2 (*red*), 3 (*blue*), and 4 (*gray*)

Due to the location of the optical access through the side windows of the SARL wind tunnel, the model needed to be elevated $1.25R$ from the floor of the wind tunnel test section in order to be positioned at the azimuth and elevation angles of interest. Furthermore, in order to maintain desirable approach boundary layer thickness ($\delta/D < 0.1$), the turret was mounted on a wall-to-wall plate (ground board, Fig. 2a). The carried vorticity of such relatively thin oncoming boundary layer predominantly rolls into a necklace vortex off the front stagnation line and has only minor effect on the prevailing dynamics of the separated flow. The design was guided by CFD simulations (not shown), which predicted the incoming turbulent boundary layer of $\delta/D \approx 0.06$. The ground board was $8.75R$ long and $5.9R$ wide and equipped with an adjustable eight-inch chord trailing-edge flap. Proximity of the board to the tunnel floor increases the pressure under the board and, left untreated, would induce a positive flow angle over its leading edge. Therefore, the flap was positioned during the initial phase of the testing in order to suppress the nonzero approach angle of the flow over the plate leading edge. The flap accelerates the flow under the board to minimize this approach flow angle. The model is located $3R$ downstream from the leading edge of the ground board.

Figure 2 also illustrates all the sensors utilized for the aerodynamic part of the flow diagnostics, which included arrays of static pressure ports distributed both on the turret surface and on the ground board. Two pairs of static pressure ports were positioned on the upper and lower leading edge of the ground board, which were used to elucidate the flow approach angle. Downstream from the turret, two orthogonal arrays, spanning $1.48 < x/R < 2.62$ ($z/R = 0$) and $-1.12 < z/R < 1.12$ ($x/R = 1.65$), were aimed at characterization of the characteristic scales of the resulting wake, where streamwise and spanwise coordinates $x$ and $z$ are measured relative to the turret center. Two inset plots in Fig. 2 further illustrate two additional static pressure domains: the flow just upstream from the optical aperture is characterized by a circumferential array of static pressure ports wrapped around the optical aperture, while a $9 \times 3$ surface array of static pressure ports is distributed on a side of the optical aperture for (segmented) spatial characterization of the flow as it becomes separated off the turret surface. Static pressure measurements through 0.5 mm ports were acquired by a Pressure Systems scanner, where the averaged pressure measurement is based on 500 individual samples. Besides the described arrays of static pressure ports, five dynamic pressure transducers were also split between the turret and the ground board. In order to characterize dynamics of the wake over the aperture, three (PD1–PD3) were distributed just downstream from the aperture (see bottom inset in Fig. 2), while the remaining two (PD4 and 5) are positioned on the ground board, just upstream from the expected wake reattachment zone (Vukasinovic et al. 2011), symmetrically about the central plane. The dynamic pressures on the ground plane and the turret were measured through standard 2–3 mm ports using a PCB 103B01 (3.33 psid) and LQ-125-5D (5 psid) transducers, respectively, that were sampled at 20 kHz, and the mean spectra of pressure fluctuations were computed using twenty spectra calculated over one-second subintervals.

To perform the aero-optical measurements, a $1.2 \times 3$ m optical table was attached to the tunnel side wall using several trusses, schematically shown in Fig. 3. A series of inner-tube tires were used to isolate the optical table from high-frequency mechanical oscillations induced by the tunnel. Optical measurements of 2-D wavefronts over the aperture of 0.254 m were performed using a high-speed Shack-Hartmann Wavefront Sensor (WFS). The schematic of the experimental optical set-up is shown in Fig. 3. A Nd:YAG laser beam was initially expanded to a 25.4 mm collimated beam and finally was expanded to a 0.254 m round beam using a 1:10 telescope. The beam was steered to the optical insert mounted on the turret. The optical insert was designed to reflect the collimated beam

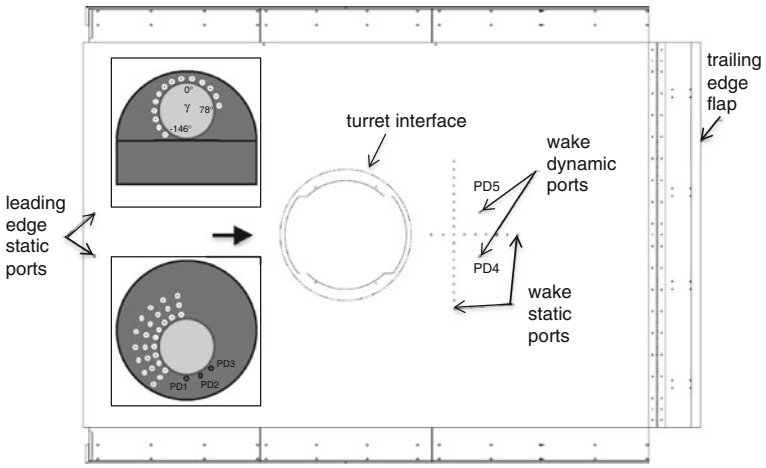


**Fig. 2** Streamwise and spanwise arrays of static pressure ports and two dynamic pressure ports (PD4 and PD5) on the ground board. *Two inset plots* show schematics of the array of static pressure ports upstream from the aperture (*top*) and a surface segment covered by $3 \times 9$ static pressure ports and three dynamic pressure ports (PD1–PD3, *bottom*)

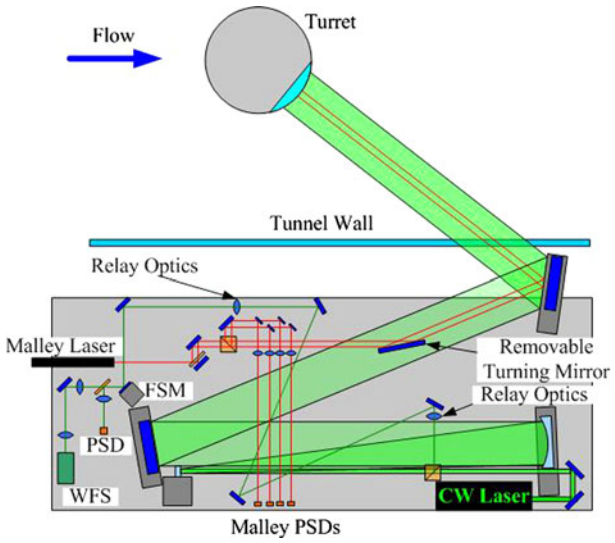


**Fig. 3** Optical diagnostics setup

as an optical flat, but a spherical curvature of outer lens was matching the turret spherical surface and the optical insert was mounted flush with the hemispherical portion of the turret. The beam was reflected by the optical insert back to the optical table along the same path it came in, passing twice through the same turbulent field and therefore increasing signal-to-noise ratio. After the beam was reduced back to the 25.4 mm beam by the 1:10 telescope, it was reflected sideways and, after passing relay optics, was re-imaged onto a closed-loop fast steering mirror (FSM) system. The FSM system was designed to reduce overall jitter imposed on the beam by the vibrating turret model and the tunnel. Finally, the beam was further compacted to a 10-mm beam and forwarded onto the high-speed WFS.

The 2-D wavefront data were acquired with a spatial $25 \times 25$ sensor grid at a sampling rate of 25 kHz; the number of frames per each run was 15,000 with a total sampling time of 0.6 s. Using all frames per each set, a steady lensing component and an instantaneous tip/tilt were removed from each wavefront. The spatial distribution of the $\mathrm{OPD_{rms}}$, defined as a temporal root-mean-squared value of *OPD* at every spatial point, was computed, along with the time-averaged spatial root-mean-squared *OPD* value over the aperture, denoted by $\overline{\mathrm{OPD_{rms}}}$. All wavefront data were normalized by $(\rho/\rho_{\mathrm{SL}})M^2D$, the normalization parameter for subsonic speeds (Gordeyev and Jumper 2010). A variance of spatial $\mathrm{OPD_{rms}}$ in time was calculated for all tested devices and viewing angles. In addition to the spatial distribution of $\mathrm{OPD_{rms}}$, cross-correlation functions, $C(\Delta x,\ \Delta y) = <OPD(x,\ y,\ t)OPD(x + \Delta x,\ y + \Delta y,\ t) >$, were calculated in the flow ($x$-axis) and the cross-flow ($y$-axis) directions.

A 4-beam Malley Probe was used as a second sensor to collect 1-D slices of wavefronts at the sampling frequency of 100 kHz and the sampling time of 30 s (see Fig. 3). In addition to wavefront data, the 4-beam arrangement allows obtaining the local convective speed by measuring time-delays between beams. To remove mechanically induced jitter from aero-optical data, the Malley probe data were collected simultaneously with four accelerometers installed on the back of the optical canister (not shown). Four-beam Malley Probe data were collected simultaneously with accelerometers at a sampling rate of 100 kHz. Two sets of data per each run were collected, each of 15 s in duration.

Prior to their integration in the model, four-jet modules of the fluidic oscillating jets were bench-tested. The jets were characterized using hot-wire anemometry, which yielded the variation of the mean velocity magnitude $U_{\mathrm{j}}$ with streamwise and spanwise position relative to the exit plane (the jet exit orifice measured $4.5 \times 1.5$ mm) and the variation of the oscillating frequency with jet flow rate. The scaled distributions of velocity magnitude are shown in Fig. 4a, b, which indicates a self-similar evolution. The corresponding oscillation frequencies (Fig. 4c) are extracted from the power spectra of the velocity fluctuations. These data indicate that, in the operation range of interest ($Q = 0{-}20$ l/min per jet), the oscillation frequency is proportional to the flow rate, and its upper bound is at about 4 kHz. As an illustration, a sample spectrum of the jet's velocity fluctuations is shown in Fig. 4d for the highest operating frequency, measured at the jet centerline and $x'/x'_{1/2} \approx 1$. The local coordinate system is tied to the center point of the jet orifice exit plane, where $x'$ and $z'$ are aligned with directions normal to the exit plane and with the long orifice side, respectively.

## 3 The baseline flow

Combinations of the aperture/turret attitudes were selected to cover the regions of the harshest optical aberrations that are realizable under the unconstrained optical paths of the laser beams through the test section optical windows. A total of six turret attitudes were tested, having combinations of the elevation and azimuth angles: (13°, 142°), (26°, 142°), (31°, 129°), (15°, 179°), (30°, 179°), and (45°, 179°). The overall turret surface coverage is illustrated in Fig. 5a, where the aperture parameter space is shown as six aperture boundaries overlaid over the base turret geometry. It should be noted that the optical aperture was not partially covered at the lowest elevation angles, as the cylindrical support had a cutout "smile" to accommodate a portion of the optical aperture. A cumulative surface area covers most of the turret aft quadrant, and by invoking the center plane symmetry, this attitude subset should be a representative of most of the aft half of the aperture orientations. Clearly, the aft half of the attitude space is of much more interest for

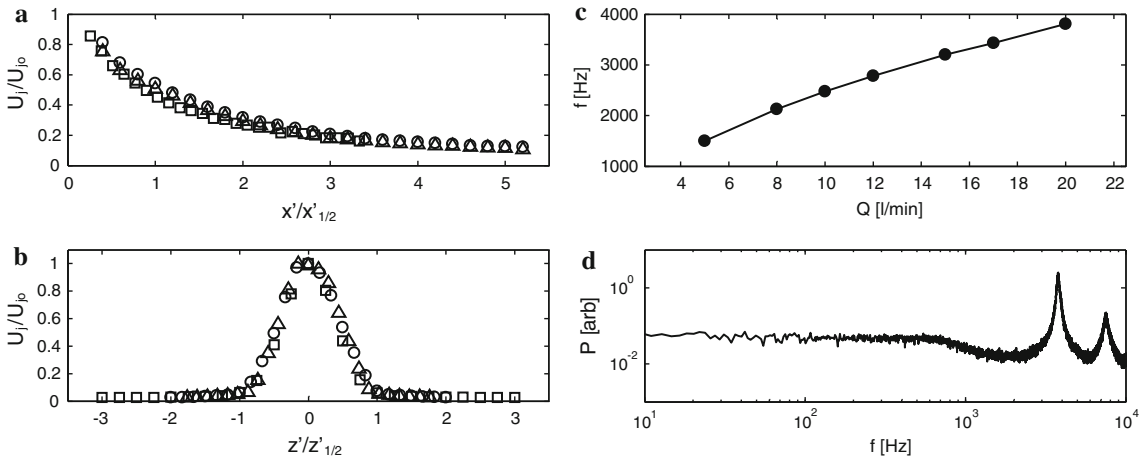


**Fig. 4** Scaled streamwise (**a**) and spanwise (**b**) velocity magnitude profiles of the oscillating jet for the jet flow rate $Q = 10$ (*circle*), 15 (*square*), and 20 (*triangle*) l/min, and the oscillating frequency with the flow rate (**c**). A sample power spectrum of the velocity magnitude fluctuations is shown in (**d**) as a reference ($Q = 20$ l/min)

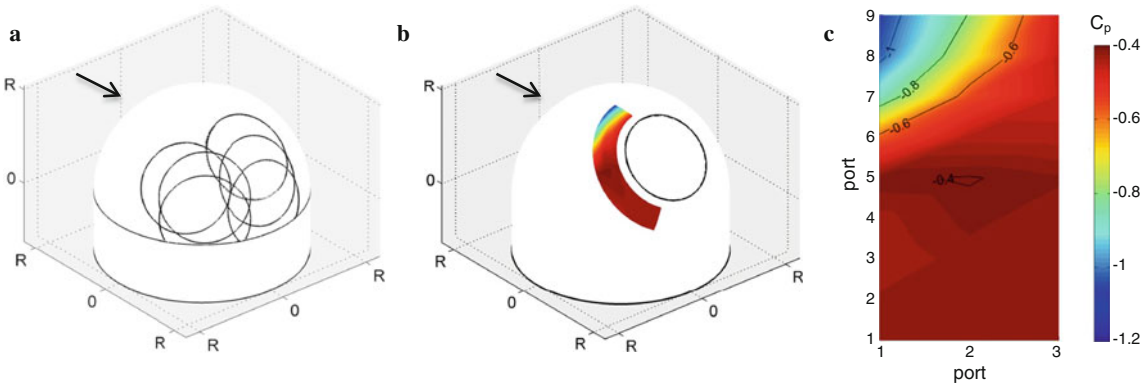


**Fig. 5** Schematics of the investigated optical aperture attitudes (**a**), and contour plots of the surface pressure distribution measured for the baseline flow (45°, 180°), overlaid on the turret (**b**) and 'unwrapped' over the 3 × 9 measured ports (**c**)

the flow control applications, as the forward space is traversed by the non-separated flow and generally should impose only a small detrimental effect on an optical passage in subsonic flows. All of the first three turret attitudes were characterized by both aerodynamic and aero-optic diagnostics. The last three attitudes, a subset of cases at nearly straight downstream looking angles (azimuthal angle 179°), were characterized only by the static and dynamic pressure measurements, as the optical passage exceeded the optical access points to the test section. The only exception was a custom-inserted optical window at the top end of the test section that enabled transmission of a Malley probe beam at turret attitude (30°, 179°).

Figure 5b, c gives an insight into the mean pressure field and the flow incipient separation off the turret surface. The measured static pressure field for the baseline flow (45°, 179°) is shown as a contour plot overlaid over the turret surface (Fig. 5b) and as an 'unwrapped' planar contour plot (Fig. 5c) that is used as a default surface plot representation hereafter. It should also be noted that the same contour color scheme ($-1.2 < C_p < -0.4$) is used in all the pressure contour plots throughout the paper. The surface pressure distribution captures the flow separation of the turret surface just upstream from the optical aperture ($C_p \approx -0.4$). Given the elevation angle of 45°, the central upstream edge of the aperture is at an elevation of about 69°, and therefore, these measurements suggest the central separation point of about 20° past the apex. Compared to the detailed central pressure profile measurements of the same scale model (Vukasinovic et al. 2011), the present baseline flow separates more than five degrees closer to the turret apex. This discrepancy is further discussed in conjunction with Fig. 6, which shows the streamwise and spanwise static pressure distributions for the baseline flows of all six aperture attitudes. Clearly, as the optical aperture is conformal, its various orientations should not have any effect on the baseline flow. This is seen in Fig. 6, but a slight scattering is present in the streamwise pressure

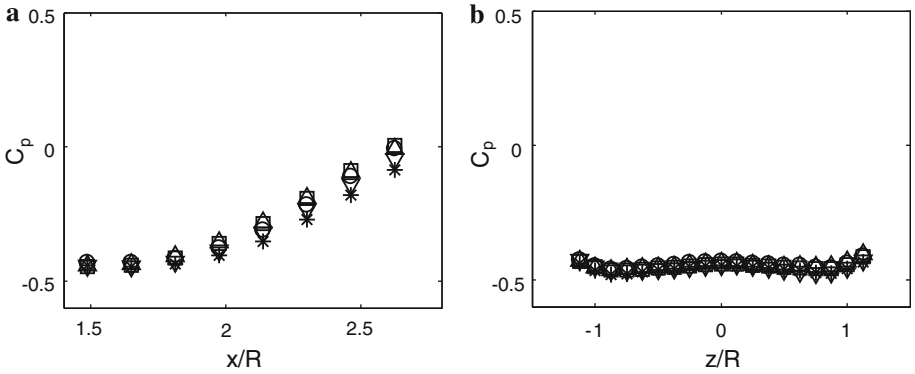


**Fig. 6** Wake axial (**a**) and spanwise (**b**) static pressure distributions for the baseline flows at the aperture elevation and azimuth angles: *open square* (15°,179°), *open circle* (30°,179°), *open triangle* (45°,179°), *open diamond* (13°,142°), *openinverted triangle* (31°,129°), *asterisk* (26°,142°)

distributions, with higher excursions closer to the wake reattachment zone. These variations are attributed to the active jets' orifices, which are present on the surface even when inactive. Each of the four zones of actuators has a common plenum, and under the sufficient pressure gradient across the plenum, there is a possibility of a cross-flow between different orifices. In order to completely eliminate any possibility of a cross-flow through the inactive jet orifices, it would be necessary to isolate each of the actuators. Another important feature of the streamwise profiles shown in Fig. 6a is that the baseline flow does not appear to reattach within the measurement domain downstream from the turret, i.e., it reattaches beyond $x/R = 2.6$. In comparison, the flow visualization done on the equivalent turret model under the same flow conditions (Vukasinovic et al. 2010a, 2011) indicated that the wake reattaches at about $x/R = 2.3$. Given the indication that the baseline flow in the present test separates off the turret surface closer to the apex (Fig. 5), it can be expected that the wake characteristic scales are larger than for the case of delayed separation, and therefore, the wake reattachment length is increased. There are several differences that could contribute to the noted differences in the present and prior baseline flows. Although the turret models are nominally the same in size, there are major differences in their positioning and support in the wind tunnel test section. As described above, the present model is mounted approximately at the test section central section, but it is elevated on the ground board, which utilized the trailing flap for adjustment of the approach flow angle. The prior model was mounted directly on the tunnel side wall in the upstream part of the test section. These differences are sufficient to introduce slight variations in the flow approach angle from one test to another, and different approach boundary layer thicknesses, although neither of these parameters were quantified in these studies.

The baseline flow dynamics was elucidated from the dynamic pressure measurements at five sensors PD1–5 (Fig. 2). Figure 7 shows the power spectra for each of the dynamics pressure fluctuations for the aperture most-downstream azimuth of 179° and the three elevation angles of 15°, 30°, and 45°. First, it should be noted that the three sensors on the turret (PD1–3) exhibit virtually identical energy distributions in all the cases, indicating a rather uniform surface dynamics behind the aperture, as they always remain deep into the separated flow. Likewise, the two ground-board sensors (PD4–5) also exhibit the same dynamics, which suggests symmetric wake dynamics across the symmetry plane. Second, as it may be expected, the total energy of surface pressure fluctuations in the vicinity of the optical aperture (Fig. 7a–c) is much lower than the corresponding energy on the ground board (Fig. 7d–e), as the former are immersed into the low-speed separated flow, and the latter presumably pick up some of the massive unsteadiness associated with the wake reattachment further downstream from the dynamic pressure locations. Although spectra for both the turret- and board-positioned sensors exhibit an inertial sub-range of energy (−5/3 slope), the two on the board represent a 'classic' fully turbulent spectra, having a clear delineation between the large and small scales, separated by a wide inertial sub-range. All the spectra have a peak at the blower blade passage frequency (156 Hz), and the ground-board spectra also show a broad peak at about 39 Hz, which is attributed to the dominant wake-mode frequency, as the corresponding Strouhal number is $St = 0.23$; similar results were reported by Gordeyev et al. (2007). This frequency is certainly influenced by several dominant modes of the wake dynamics including, perhaps, sinuous and varicose mode. Figure 7a–c shows a consistent shift of increasing energy of pressure fluctuations with a decrease in the elevation angle, as the pressure fluctuations increase with an increase in the recirculating flow intensity along the turret surface, away from the flow separation line. The pressure fluctuations on the ground board are unaffected by the turret elevation change as the wake flow is independent of the orientation of the conformal optical aperture. As it was confirmed in all of the tested cases, the three dynamic pressure sensors indicate equivalent surface pressure dynamics, only pressure PD3 is chosen to be shown

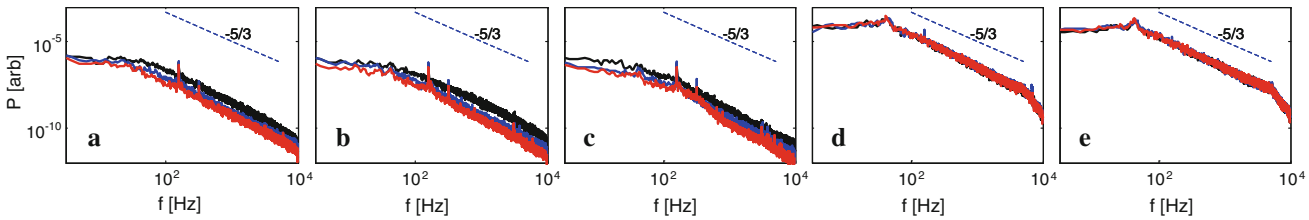


**Fig. 7** Power spectra of the pressure fluctuations measured by the sensor: PD1 (**a**), PD2 (**b**), PD3 (**c**), PD4 (**d**), and PD5 (**e**) for the baseline flow at aperture azimuth angle $\beta = 179°$ and elevation angles $\alpha = 15°$ (*black*), 30° (*blue*), and 45° (*red*)

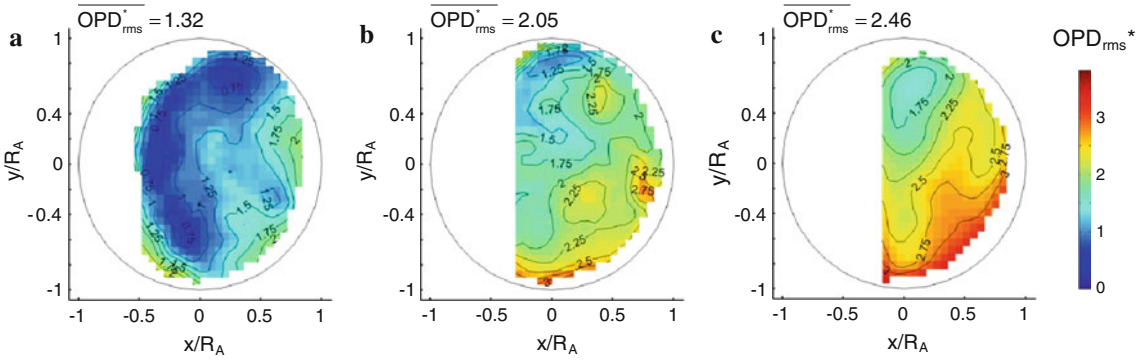


**Fig. 8** Spatial distribution of normalized $OPD_{rms}$ for the baseline flow turret attitudes: **a** (31°,129°), **b** (26°, 142°), and **c** (13°,142°). Flow goes from *left* to *right*

hereafter, as a representative for the near-aperture dynamics. Likewise, only PD4 is chosen as a representative for the pressure dynamics on the ground board.

Spatial distributions of $OPD_{rms}$ for baseline cases at different aperture attitudes are shown in Fig. 8, as measured by the 2D high-speed Wavefront Sensor (Sect. 2). Note that wavefronts were measured over a partial area of the aperture, due to clipping effects of the test section support beams and, sometimes, due to clipping caused by the steering mirrors. Flow is from left to right. At (31°, 129°), the flow begins to separate over the upstream portions of the optical aperture, but the aperture is sufficiently upstream and elevated, such that it does not direct the beam directly through the 'horn' vortex. As a result, the normalized $OPD_{rms}$ is the lowest out of all the three off-center turret attitudes. As the azimuth angle is increased to 142° and elevation slightly lowered to 26° (Fig. 8b), the flow over the aperture is fully separated, having progressively increased levels of aberrations from left to right, as the separated region grows. Furthermore, lowering of the elevation angle brought the aperture to increased direct exposure to the 'horn' vortex, which also increases the level of aberrations at the aperture bottom. Finally, as the azimuthal angle stayed fixed and the turret elevation was lowered to only 13° (Fig. 8c), the 'horn' vortex direct influence spread over a wider area of the aperture lower section. This, in turn, increased the levels of optical aberrations across the lower portion of the aperture, resulting in the highest overall aberrations of the normalized $OPD_{rms} = 2.46$ over the measurement domain.

## 4 Characterization of the controlled flow

### 4.1 Turret near-center attitudes

A subset of tests was done for the near-center plane orientations (azimuth angle of 179°), having aperture elevation angles between 15° and 45°. The resulting baseline and controlled flows were primarily characterized by the pressure measurements, except at the elevation of 30°, which was also characterized aero-optically by the Malley probe measurements.

Once the optical measurement at a given orientation was completed, the optical aperture was replaced by an instrumented conformal cap that had nine static pressure ports along its symmetry line, which were connected to the data acquisition system by disconnecting the nine most-downstream static pressure ports in the surface pressure array, as schematically shown in Fig. 9a. This switch was done in order to further investigate discrepancy in the baseline flow separation angles between the current and previous studies (Vukasinovic et al. 2010a, 2011). The measured pressure profiles across the aperture replacement

cap are shown in Fig. 9b for the baseline flow (line) and active control (open symbols), and in Fig. 9c, for the baseline flow (line), passive (open symbol), and hybrid (solid symbol) control. In addition, the corresponding pressure profiles (Vukasinovic et al. 2011) are overlaid for reference. All the current baseline profiles collapse onto the same $C_p \approx -0.4$, indicating the flow is separated for all the elevation angles. The shift in the separated flow $C_p$ from the prior test is in accord with other indications that the baseline flow remained attached further in earlier studies; not only that the reference profile indicates the center plane separation at elevation of about 63°, but the separation $C_p$ is, consequently, at higher level of $C_p \approx -0.3$. For the active control cases, only the highest elevation angle port locations captured the flow separation; for the active flow control only by the Zone 1 actuators at $C_\mu = 1.3 \times 10^{-3}$, the flow separates at the centerline at an elevation of about 50°. Although the exact separation point for the baseline flow was outside of the pressure ports range, it can be stated that the active flow control in this case induced a separation delay of at least 15° in the central plane. Both passive and hybrid control cases (Fig. 9c) indicate even more pronounced effectiveness on the flow separation delay. Passive control seems to both delay the separation up to the elevation of about 60° and accelerate the flow over the turret (note the $C_p$ dip to below −0.5 at separation). Furthermore, once separated, the flow may reattach again, as the pressure level begins to recover below about 25° elevation. Similar trends are seen in all the hybrid control cases, as initially delayed separation is always followed by a secondary pressure recovery, which may be also associated with the recirculating flow near the juncture between the turret and the ground board. It also appears that the separation delay is inversely proportional with the turret/aperture elevation angle, as initial separation is delayed from about 55° to 45° for a change in the aperture elevation from 45° to 30°. A significant pressure recovery for the aperture elevation 15° is in accord with further separation delay with a decrease in the aperture elevation angle.

The main reason for having a relatively large surface area population by the control jets is a large range of the aperture attitudes, and in particular, incorporation of very low aperture elevation angles. Depending on a particular turret attitude, a combination of the active control zones is selected, and all of the four control zones are never set active simultaneously. It should be noted that operation of the most upstream control jets far into the attached flow (i.e., upstream of separation) could also result in adverse effect on the aerodynamics and aero-optics environment around the turret. Some examples of the aerodynamic control effect relative to the $C_\mu$ and active control zones are shown in Fig. 10 in terms of the pressure profile upstream from the aperture. The pressure ports orientation is defined by the local angle $\gamma$, relative to the optical aperture, where $\gamma = 0°$ coincides with the aperture vertical symmetry plane (see inset schematics in Fig. 2). This example, for the turret attitude (45°, 179°), shows different actuation flow rates for the active (Fig. 10a) and hybrid (Fig. 10b) control approaches. When utilizing only the flow control actuators in Zone 1 (closest to the optical aperture), the actuation effect follows the intuitive expectation that an increase in the flow rate would result in further separation delay. As the approach flow to the aperture is fully separated (nearly constant $C_p \approx -0.4$), the active control is capable of recovering the attached flow about the center plane, and the reattached zone widens with an increase in $C_\mu$. However, if actuation Zones 1, 2, and 3 are utilized at the highest flow rate, there is virtually no effect on the separation, partially because the flow control is activated over Zones 2 and 3

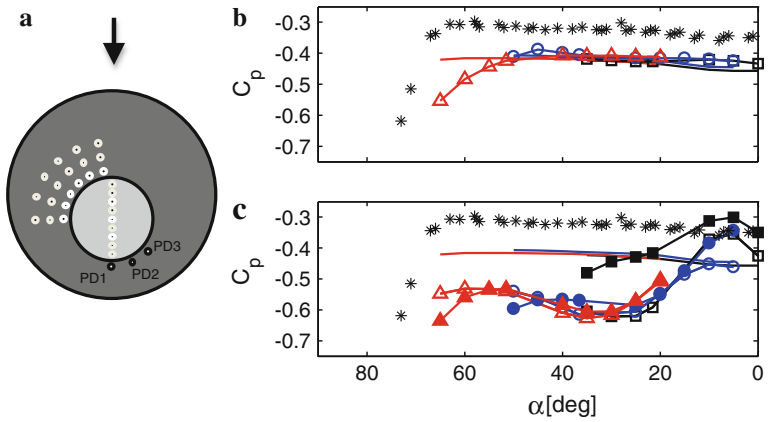


**Fig. 9** **a** Schematics of the nine static pressure ports redistributed to the optical aperture cap. Static pressure distributions for the turret azimuth angle $\beta = 179°$ and three elevation angles $\alpha = 15°$ (*black*), 30° (*blue*), and 45° (*red*). **b** Baseline (*line*) and active control cases for $C_\mu \times 10^3 = 1.3$ (*open circle*, *open triangle*) and 2.1 (*open square*). **c** Baseline (*line*), passive (*open symbols*) and hybrid control cases for $C_\mu = 1.3 \times 10^{-3}$. The corresponding pressure profile (*asterisk*, Vukasinovic et al. 2011) is shown for reference

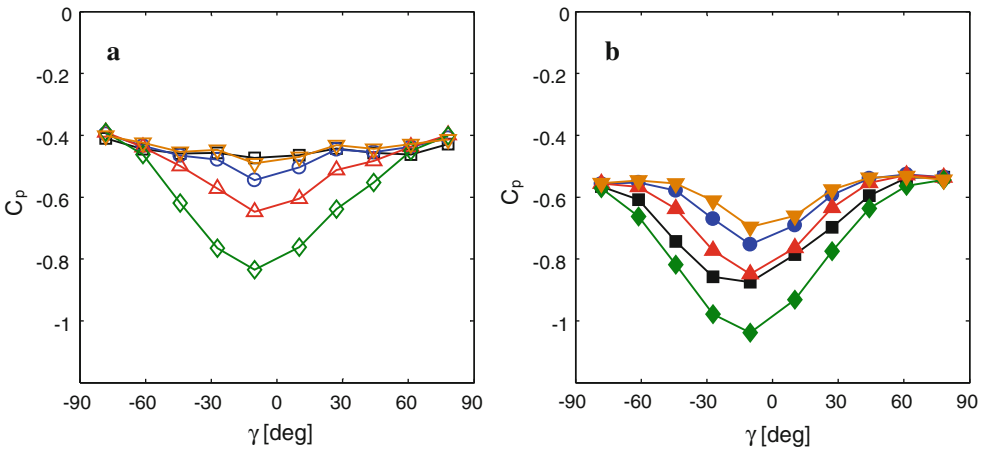


**Fig. 10** Static pressure profiles upstream from the optical aperture (45°, 179°) for the baseline flow (*open square*), passive (*filled square*), and fluidic control at $C_\mu \times 10^3 = 0.9$ (*open circle*, *filled circle*, Zone 1), 1 (*open triangle*, *filled triangle*, Zone 1), 1.3 (*open diamond*, *filled diamond*, Zone 1), and 1.5 (*open inverted triangle*, *filled inverted triangle*, Zones 1, 2, 3), for the active (**a**) and hybrid (**b**) control schemes

that are far upstream into the attached flow, and in part because the flow control effectiveness of Zone 1 is lowered, as Zones 2 and 3 each contribute to 20 % of the effected $C_\mu$. The passive control significantly accelerates the outer flow around the turret and delays the flow separation (Fig. 10b), as the flow just upstream from the aperture becomes fully attached ($-0.55 < C_p < -0.85$). This global flow alteration essentially renders even the most upstream rows of actuators in Zone 1 immersed into the attached flow. As a consequence, running the Zone 1 actuation at lower actuation flow rates in hybrid configuration actually has a detrimental effect on the separation relative to the passive control, until the highest flow rate is attained, which constitutes the best hybrid flow control configuration for that turret orientation. These findings also indicate that even further improvement in the hybrid flow control effectiveness could be attained by actually reducing the number of active control jets, i.e., by deactivation of the most upstream rows of Zone 1, which was not possible under the current flow control segmenting.

Further comparison among the active, passive, and hybrid flow control aerodynamic effects for the turret orientation (45°,179°) is shown in Fig. 11 in terms of the static pressure characterizations. The 'unwrapped' surface contour plots are shown in Fig. 11a–d, for the baseline, active, passive, and hybrid control, respectively. It is seen that the baseline flow separates first on the aperture (turret) side and that the separation line progressively advances in the downstream direction, and the flow stays attached farthest at the apex. This separation line progression across the turret surface is in accord with the previous studies (Vukasinovic et al. 2010a, 2011). It is also shown that the flow is already fully separated before approaching the outer boundary of the optical aperture ($C_p \approx -0.4$). The corresponding axial (Fig. 11e) and spanwise (Fig. 11i) pressure distributions indicate that the wake is open in the whole measurement domain, i.e., it does not reattach up to $x/R = 2.6$. Once the active control is applied, surface flow becomes accelerated, predominantly over the apex region (Fig. 10b), which is indicated by the lowered $C_p$ that extends almost up to the optical aperture edge. Consequently, this would indicate that the flow separation is delayed. The pressure distributions in the axial and spanwise directions (Fig. 11f, j) indicate a favorable, but not significant effect of the active control on the global wake topology. Contrary to this case, the passive control induces a rather dramatic suppression of the wake extent (Fig. 11g, k), where the wake reattachment in the central plane is forced down to $x/R \approx 1.9$. The pressure surface contour plot shows that the accelerated flow extends both in the spanwise and streamwise directions over the turret and reattaches along the whole approach edge of the optical aperture. An addition of the active control to the passive control, in hybrid configuration, shows an incremental improvement relative to the passive control in both the further extension of the lowered surface pressure upstream from the optical aperture (Fig. 11d), and in the wake suppression (Fig. 11h, l).

As already outlined in Sect. 2, only a single-point aero-optical measurement using a Malley probe was feasible at near-center plane, by making a special optical provision in a tunnel wall for the aperture attitude (30°, 179°). It was found that the active control resulted in the highest suppression of aero-optical aberrations, and the deflection power spectrum for the control effected by the jets closest to the aperture at $C_\mu = 1.4 \times 10^{-3}$ is plotted in Fig. 12a, along with the baseline power spectrum. The convection speed was found to be constant over the aperture, indicated by a constant-slope line in the phase of the cross-correlation between the beams for frequencies below 4 kHz (Fig. 12b), so $OPD_{rms}$ values can be calculated from deflection-angle time series. The controlled flow exhibits a broadband reduction in optical aberrations outside of the vibration-contaminated data ($St > 1.5$). The overall reduction of $OPD_{rms}$ relative to the baseline was 38 %.

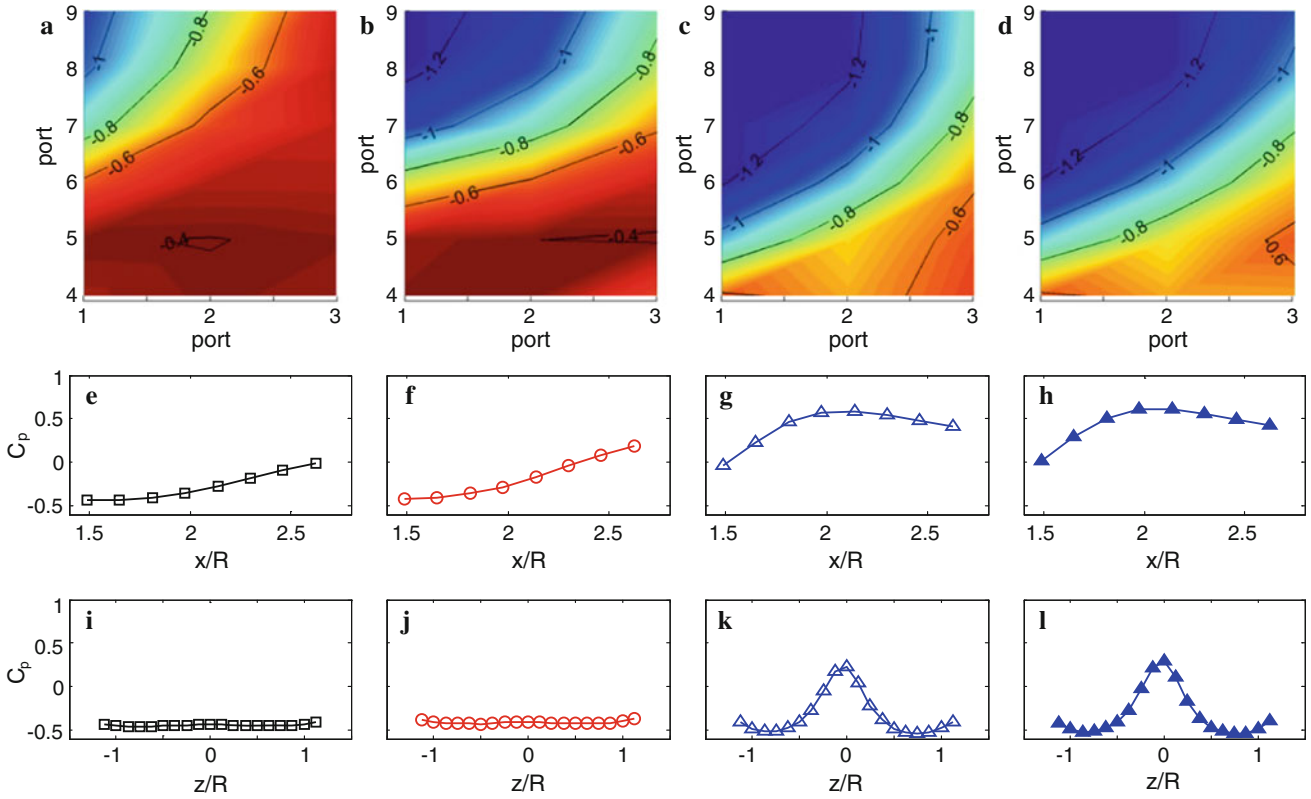


**Fig. 11** Surface pressure contour $C_p$ plots (**a**–**d**), and the wake downstream (**e**–**h**) and spanwise (**i**–**l**) profiles for the baseline (**a**, **e**, **i**), active (**b**, **f**, **j**), passive (**c**, **g**, **k**), and hybrid (**d**, **h**, **l**) control cases; $C_\mu = 1.3 \times 10^{-3}$ (Zone 1). Turret aperture attitude is (45°, 179°)

### 4.2 Turret off-center attitudes

A number of investigations of the flow over a turret have shown that the separated flow is dominated by two 'horn' vortices (e.g., Gordeyev and Jumper 2010). Therefore, it is expected that the most challenging aero-optical environment includes off-center azimuth angles, such that the optical beam traverses those vortices along its path. The present investigation focuses on three such turret attitudes, as illustrated in Fig. 5a.

Although the hybrid flow control approach, in principle, nominally showed the most effectiveness in achieving both aero-optical and aerodynamic flow improvements, the actuation for the turret attitude that included the lowest elevation angle of 13°, combined with the azimuth 142°, encountered a couple of detrimental effects related to the proximity of the passive plate to the optical aperture: shedding of the plate-generated vorticity directly over the aperture and, in some instances, by direct interference of the plate tail and the aperture. Therefore, at such turret attitudes, the active control was the most effective control approach, although it is expected that by introduction of adjustable plate height to eliminate the plate-aperture interference, the properly adjusted hybrid flow control would achieve the highest effectiveness even at the low elevation angles. Figure 13 presents the aerodynamic characterization of the active flow control effect for the turret orientation (13°, 142°). A difference between the active control case ($C_\mu = 1.8 \times 10^{-3}$, Zones 1–3) and the baseline flow is represented by the all three static pressure characterizations. The wake diagnostics (Fig. 13a–b) shows that the actuation favorably effects the wake recovery, although not significantly. It is interesting to note how the active control breaks the wake symmetry about the centerline (Fig. 13b) as the actuation is applied asymmetrically relative to the center plane, due to the turret aperture 142° azimuth orientation. Pressure profiles upstream from the aperture (Fig. 13c) show that the flow is fully separated over most of the measurement domain ($C_p \approx -0.4$) for the baseline flow (Fig. 13d). As the flow control is applied, the flow remains attached at the upper subset of the measurement domain, where the flow eventually separates just upstream from the aperture boundary; no significant change is effected over the surface area closer to the cylindrical support, as that area is not populated by the control actuators (see Fig. 1b).

Additional insight into the active flow control effect shown in Fig. 13 is gained by the analysis of the corresponding dynamic pressure sensor measurements. The representative controlled and uncontrolled spectra of the

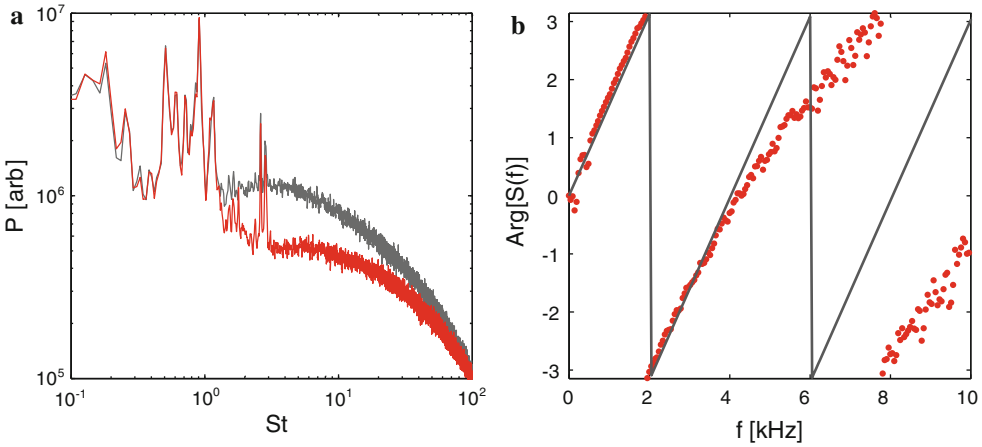


**Fig. 12** **a** Malley Probe deflection-angle spectra for the baseline (*gray*) and the active control case by Zone 1 ($C_\mu = 1.4 \times 10^{-3}$) for the turret attitude (30°, 179°). **b** The phase of the cross-correlation spectral function between Malley probe beams for the baseline flow

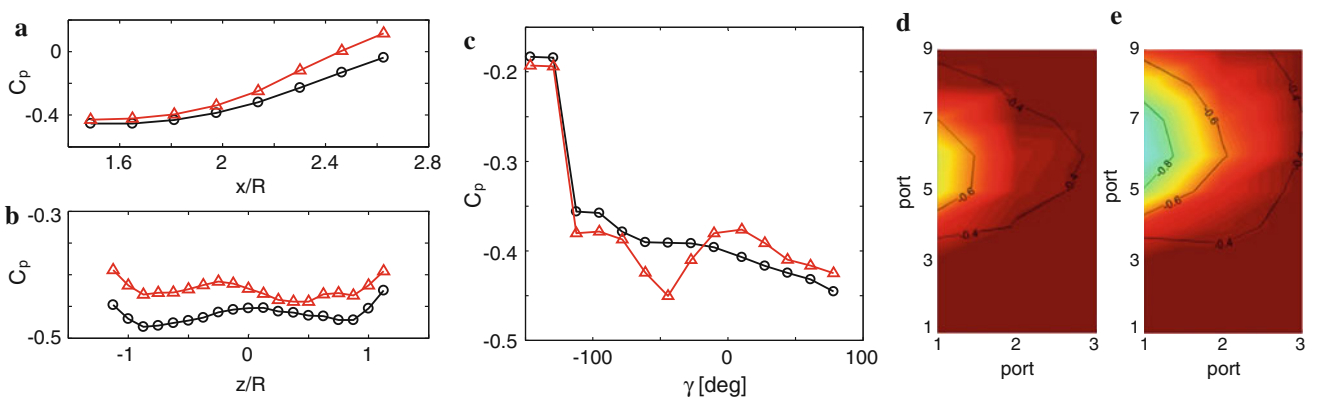


**Fig. 13** Static pressure: wake downstream (**a**) and spanwise (**b**) profiles, upstream from the optical aperture (**c**), and surface pressure contour plots for the baseline flow (*open circle*, **d**) and active control (*open triangle*, **e**) at $C_\mu = 1.8 \times 10^{-3}$ (Zones 1, 2, 3). Turret aperture attitude is (13°, 142°)

surface pressure fluctuations on the turret (PD3) and on the ground board (PD4) are shown in Fig. 14. A signature of the 'high-frequency' flow control (Vukasinovic et al. 2010b) measured on the velocity field fluctuations (Vukasinovic and Glezer 2007; Vukasinovic et al. 2010a) is suppression of the energy-bearing velocity fluctuations across most of the wake's shear layer. A similar effect is seen here in terms of a broadband reduction in the energy of surface pressure fluctuations behind the optical aperture. It is conjectured that these effects on the velocity and pressure fields are coupled. The turret surface pressure dynamics is important as it couples to its unsteady loading and buffeting that could be another significant indirect source of optical aberrations due to structural vibrations, in addition to the direct aerodynamic aberrations that result from the flow field traversed by the optical beam. A less prominent effect is seen in the 'far field' pressure fluctuations on the ground board (Fig. 14b), although it can be argued that the changes on the global wake topology and its dynamics are in accord with the previous findings that the active flow control does not significantly delay the flow separation (Fig. 13) for this turret attitude. Therefore, its effect on the far field surface pressure dynamics is more subtle, but it does reduce energy of the large-scale pressure fluctuations, and appears to somewhat shift the dominant wake-mode frequency from Strouhal number 0.23 to 0.29, which implies reduced scales of the dominant wake structures.

The corresponding aero-optical results, measured by the 2D wavefront sensor, are shown in Fig. 15. It is seen that the active flow control separation delay at the top of the aperture (Fig. 13d), which combined with the suppressed level of pressure (and implied velocity) fluctuations, consequently improved the overall $\mathrm{OPD_{rms}}$ over the aperture by 10 % for the $C_\mu = 1.8 \times 10^{-3}$ through Zones 1, 2, 3. As already discussed above, it is expected that using the adjustable passive plate as a passive component in a hybrid flow control configuration would further augment the favorable effect demonstrated by the active control.

The other two turret attitudes in off-center plane configurations have elevation angles higher than 20°, and no major detrimental interference between the passive plate

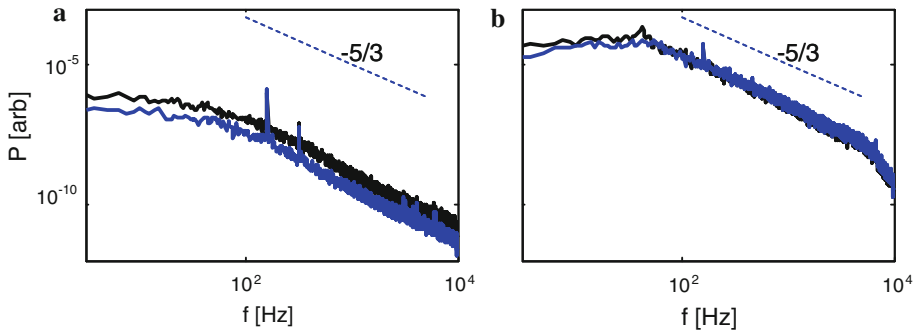


**Fig. 14** Power spectra of the pressure fluctuations measured by the sensor: PD3 (**a**) and PD4 (**b**) for the baseline flow (*black*) and the active control (*blue*) case shown in Fig. 13

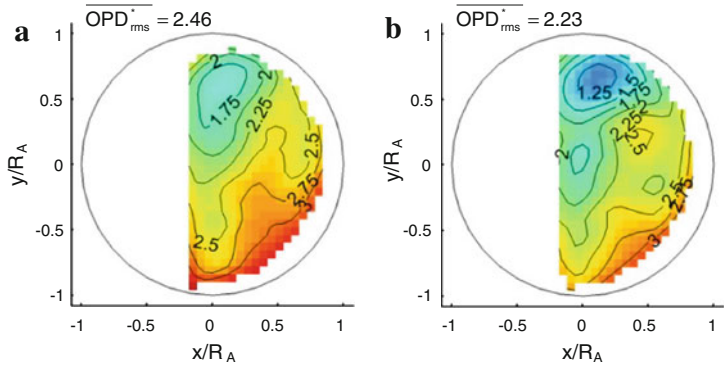


**Fig. 15** Spatial distribution of normalized $OPD_{rms}$ for baseline flow (**a**) and the flow control case (**b**) shown in Fig. 13. Flow goes from *left* to *right*

and the aperture was detected. Hence, the most effective flow control was measured in hybrid configuration for both of these turret attitudes. The resulting pressure characterization is shown in Fig. 16 for the baseline flow (31°, 129°) and the hybrid flow control including Zones 1, 3, and 4. A significant suppression of the turret wake is seen in both the streamwise and spanwise static pressure profiles. The controlled wake reattaches in the central plane at about $x/R = 2$, and it also appears to be symmetric about the center plane (Fig. 16a–b). The baseline flow just upstream from the optical aperture (Fig. 16c) is already separated over the outer sides. The controlled flow is accelerated beyond the baseline flow and fully recovers the attached flow at the aperture circumference. The pressure surface contour plots further emphasize extended favorable effect of the hybrid flow control in keeping the flow accelerated over the measured surface domain, which implies that the separation is delayed further downstream. Further consequences of the significant alteration of the flow separation and of the ensuing turret wake are seen in the representative spectra of surface pressure fluctuations on the turret (Fig. 17a) and on the ground board (Fig. 17b). Opposite to the active flow control case at the lower aperture elevation (Fig. 14a), spectra of the hybrid flow control indicate a broadband increase in the surface pressure fluctuations behind the optical aperture. This can be attributed to the delayed separation and significantly suppressed wake domain that increases the wake-bound circulation and hence increases the level of surface pressure fluctuations over the turret dynamic pressure sensors. An increase in surface pressure fluctuations over the aperture was directly measured by Palaviccini et al. (2011) and Wallace et al. (2011) in a case of the controlled separation delay and suppression of optical aberrations, respectively. The groundboard dynamic sensor PD4 is positioned just after the reattachment region in the controlled flow, and its spectra indicate several differences relative to the baseline spectra: there is an increase in the energy of the large-scale fluctuations, and also an extension of scales that carry a large energy content, all of which is attributed to the neighboring wake reattachment. In addition, as the flow reattaches and begins to regrow a new boundary layer flow, the pressure fluctuations, although rich in scales, do not follow the turbulent scaling anymore. It is interesting to note that the energy distribution of small scales, though, approaches that of the baseline flow.

The effectiveness of the hybrid flow control for this turret attitude is surmised from the high-speed measurements of partially clipped wavefronts for the baseline and the flow control case discussed in Figs. 16 and 17. Figure 18 shows the spatial distributions of normalized $OPD_{rms}$ for the baseline and the controlled case. As the baseline flow begins to separate over the upstream boundary of the aperture, and the aperture is sufficiently far away from the direct influence of the 'horn' vortex, aero-optical effects are mostly dominated by the growing shear layer in the separated flow. Therefore, the aberrations progressively increase from left to right, in the flow direction. The controlled flow (Fig. 18b)

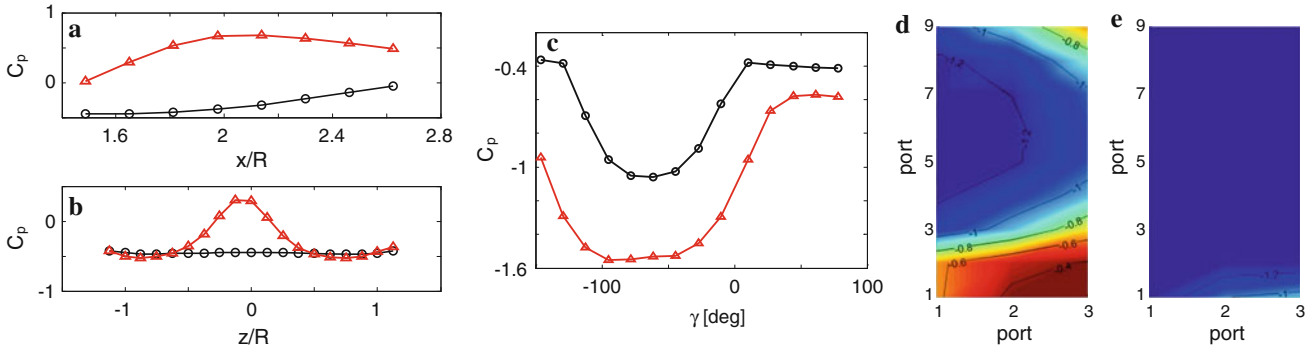


**Fig. 16** Static pressure: wake downstream (**a**) and spanwise (**b**) profiles, upstream from the optical aperture (**c**), and surface pressure contour plots for the baseline flow (*open circle*, **d**) and hybrid control (*open triangle*, **e**) at $C_\mu = 1.8 \times 10^{-3}$ (Zones 1, 3, 4). Turret aperture attitude is (31°, 129°)

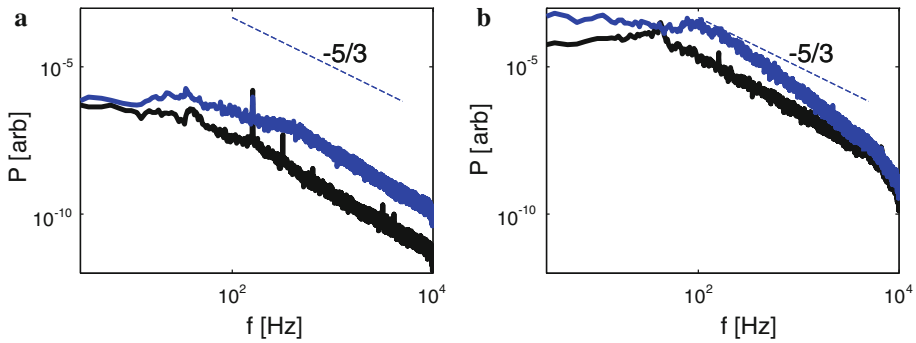


**Fig. 17** Power spectra of the pressure fluctuations measured by the sensor: PD3 (**a**) and PD4 (**b**) for the baseline flow (*black*) and the hybrid control case (*blue*) shown in Fig. 16

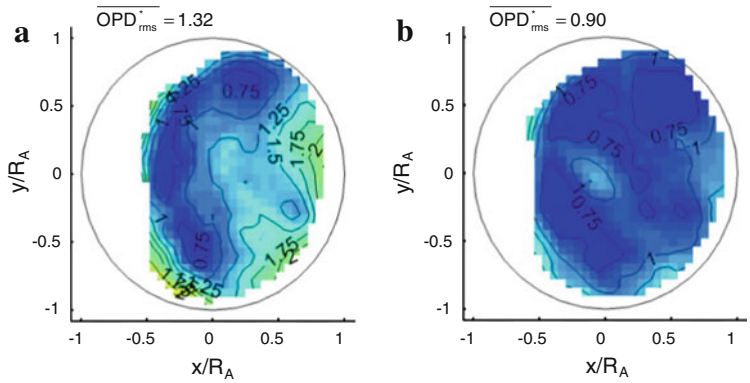


**Fig. 18** Spatial distribution of normalized $OPD_{rms}$ for baseline flow (**a**) and the flow control case (**b**) shown in Fig. 16. Flow goes from *left* to *right*

exhibits a much more uniform level of optical aberrations within the measured domain, eliminating their increase in the downstream direction, which is attributed to the separation delay implied from the surface pressure distributions seen in Fig. 16e. As a consequence, a 30 % aero-optical improvement was measured over the aperture domain. It should be noted that this overall improvement is achieved despite a notable increase in energy of the surface pressure fluctuations that were measured just downstream from the aperture (Fig. 17a). If such an effect is induced over the aperture itself, it would have a near-surface detrimental effect on optical aberrations.

Perhaps the most prominent hybrid flow control effect is seen in Fig. 19, for the turret attitude (26°, 142°). Similar to the hybrid flow control case at (31°, 129°), the wake reattaches immediately downstream from the turret, at about $x/R = 1.9$ (Fig. 19a). The baseline flow around the aperture upstream edge is almost fully separated ($C_p \approx -0.4$), and the hybrid flow control remarkably recovers the attached flow leading to the optical aperture (Fig. 19c) by accelerating the flow over the aft portion of the hemispherical cap and consequently lowering the pressure coefficients down to $C_p = -1.4$. The best representation of the remarkable effect that the flow control has on the flow over the turret is seen in comparison between the surface pressure contour plots for the baseline (Fig. 19d) and controlled (Fig. 19e) flow, where the central separated flow region becomes fully attached. The

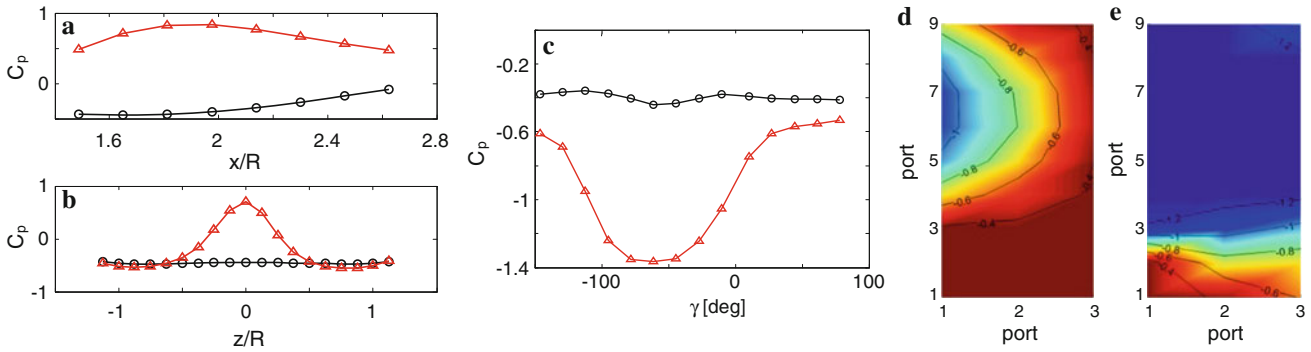


**Fig. 19** Static pressure: wake downstream (**a**) and spanwise (**b**) profiles, upstream from the optical aperture (**c**), and surface pressure contour plots for the baseline flow (*open circle*, **d**) and hybrid control (*open triangle*, **e**) at $C_\mu = 2.2 \times 10^{-3}$ (Zones 1, 3, 4). Turret aperture attitude is (26°, 142°)

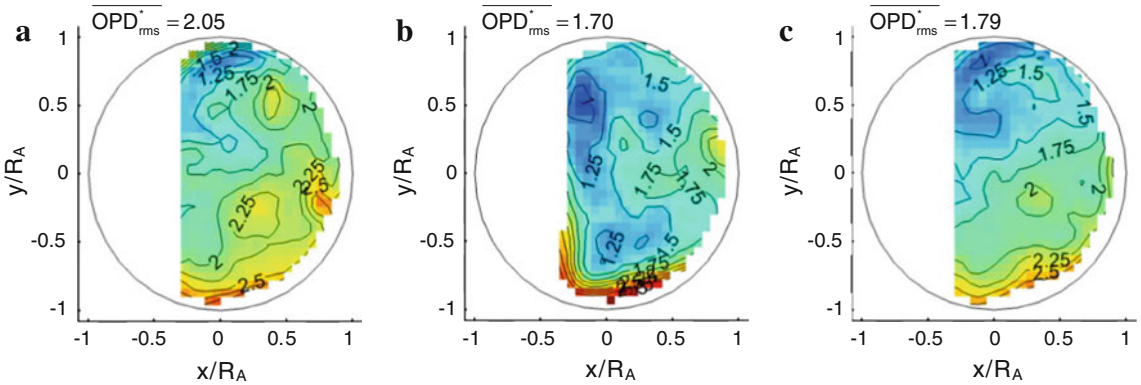


**Fig. 20** Spatial distribution of normalized $OPD_{rms}$ for baseline flow (**a**), and hybrid (**b**) and active (**c**) flow control cases for the flow condition of Fig. 19. Flow goes from *left* to *right*

remnants of the separated flow are visible only at the very bottom of the contour plot, which is not covered by the actuators, and it is below the optical aperture as well. The corresponding dynamic pressure analysis yields analogous power spectra of surface pressure fluctuations to those shown in Fig. 17 (and it is omitted for brevity), where the hybrid control increases the near turret surface pressure fluctuations, and the post-reattachment zone on the ground board exhibits an increased level of large-scale pressure fluctuations.

The results of the aero-optical characterization by the 2D wavefront sensor are shown in Fig. 20 for the baseline and the hybrid flow control. The effects of active control alone are also shown for reference. When comparing the overall aero-optical effect of the hybrid flow control (Fig. 20b) relative to the baseline flow (Fig. 20a), a significant suppression of optical aberrations is seen over most of the aperture, except at the very bottom. The large suppression of optical aberrations is in accord with conclusions based on the aerodynamic analysis (Fig. 19), while a sharp increase in optical aberrations measured at the aperture bottom is attributed to the detrimental effects from

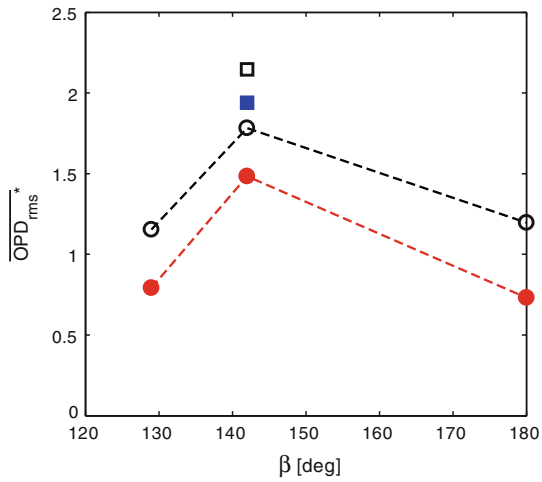


**Fig. 21** Comparison between mean normalized $OPD_{rms}$ for the baseline flow (*open symbol*) and the best flow control case as a function of a turret attitude: elevation angle $\alpha = 13°-15°$ (*square*) and 26°−31° (*circle*)

the partition plate vortex shedding. This detrimental effect lowers the overall effectiveness of the hybrid flow control configuration, but aero-optical distortions were still found

to be reduced by 16 % over the whole aperture. To test that this detrimental effect associated with the passive plate, the best active control case is shown in Fig. 20c. Active control alone significantly delayed the separation over the turret, but it lacks the depth across the whole aperture area of the hybrid control. Still, as no detrimental effect is exerted at the aperture bottom, the active control results in an overall suppression of $OPD_{rms}$ of about 12 %. It should be noted that this case also indicates that when the partition plate is positioned at the full cylinder height, this turret elevation angle is very close to the cutoff above which the detrimental plate effects would not interfere with the optical aperture in off-center orientation. Furthermore, a slight lowering of the partition plate in the present turret attitude would also bypass the plate's unsteady shedding over the aperture and, consequently, should further increase the flow control effectiveness.

Figure 21 summarizes all of the aero-optical results. If a turret attitude combines low aft elevation angles and an off-center azimuth, the optical beam passes not only through the separated flow, but it is also affected by the 'horn' vortex. Therefore, these attitudes result in the highest optical aberrations and are, in general, the most challenging to control. Both active and hybrid control at these off-center attitudes resulted in overall suppression of optical aberrations between 10 and 16 %. In comparison, for near-center turret attitudes, this study supports prior findings (Vukasinovic et al. 2010a, 2011) that significant control authority can be attained in suppression of optical aberrations. The aberrations in this region are dominated by the growing shear layer of the separated wake. The present results indicate significant flow separation delay and the resulting suppression of optical aberrations up to 40 %.

## 5 Conclusions

The effectiveness of hybrid (passive/active) flow control approaches for mitigation of aero-optical aberrations was investigated in the flow over a bluff-body model of a nominal airborne turret (0.61 m diameter hemispherical cap supported on a matching 0.19 m high cylinder) at $M = 0.3$, and $Re_D = 4.46 \times 10^6$. The model is equipped with a 0.254 m diameter conformal optical aperture/mirror assembly, which was used for direct optical characterization of the adjacent aero-optical environment. The primary optical diagnostic tool was a high-speed 2D wavefront sensor capable of simultaneous, temporal and spatial assessment of the aberrations dynamics. Temporally resolved aberrations along the beam paths were concomitantly measured using a four-beam Malley probe. The aero-optical measurements were accompanied by the measurements of the pressure distributions over the turret surface and on the support plane. Active control was effected using arrays of fluidic oscillating jets distributed upstream from the optical aperture. The control authority of the actuators was significantly enhanced using a passive horizontal partition plate that partially wrapped around the hemisphere-cylinder juncture.

The present investigation considered optical aperture attitudes that led to high degradations of the emitted/reflected optical beam by the separated flow, and therefore, only aft-pointing attitudes were considered (six attitudes were realized in the test section). The aberrations in the baseline flow exhibited two predominant features. At higher aperture elevation angles (higher than about 30°), the aberrations grew across the aperture in the direction of the prevailing flow and were attributed to flow separation and the incipient formations and growth of the separated shear layer. At lower aperture attitudes an increase in the levels of aberrations at the lower edge of the aperture was attributed to the presence of two dominant 'horn' vortices that separate off the turret surface and the interception of their path with the optical beam.

The present investigation focused on a hybrid, passive/active flow control approach. Passive control was accomplished by the addition of a simple forward-protruding partition plate at the juncture between the hemispherical cap and its cylinder support. The plate effectively decoupled the wake flow of the hemisphere from the necklace vortices at the ground plane juncture of the cylinder, and to some extent from the wake of the cylinder itself. The global alteration of the flow around the turret led to a significant delay in separation over the hemisphere by exploiting the downwash associated with the partition's own "tip" vortices and the displacement of the front stagnation line. More importantly, these changes in the global flow helped to enhance the effectiveness of direct, small-scale actuation that was effected by arrays of oscillating jets upstream from the aperture. The hybrid control led to up to 45 % reduction in the streamwise extent of the turret's wake as the separated flow attached to the ground plane less than half the turret diameter downstream from the turret. While jet actuation alone leads to broadband diminution of the spectral components of the surface pressure fluctuation downstream of the aperture as a result of the dissipative effects of the actuation, hybrid control (in the presence of the partition plate) results in a broadband increase in pressure fluctuations owing to an intensification of the recirculation within the reduced, closed wake.

Measurements of spatially and temporally averaged optical path difference (*OPD*) using a high-speed Shack-Hartmann wavefront sensor and a Malley probe over a range of turret attitudes demonstrated that the hybrid flow control led to an overall suppression of 10–40 % in aero-optical aberrations. At the lowest aperture elevation angles, the streamwise vorticity generated by the partition plate

was advected over a segment of the optical aperture, and therefore, the most effective control was produced by the jet actuation alone. However, the present investigations indicate that further optimization of the plate position/geometry would enable realization of the full benefits of hybrid flow control even at low aperture elevation angles. Hybrid flow control outperformed the passive- or active-only configurations for all turret attitudes at elevation angles higher than about 20°. The degree of aero-optical improvements depended on the dominant flow-induced aberration sources within the controlled domain. In the regions where the aberrations were dominated by boundary layer separation under a strong adverse pressure gradient, the intense vorticity concentrations associated with the evolution of a shear layer were the main source of the optical aberrations. The formation and advection of aft 'horn' vortices resulted in strong, localized three-dimensional separation and optical aberrations when the optical aperture's attitude was aligned with these vortices. This local flow separation and vorticity dynamics was less receptive to the present flow control approach that was optimized for separation control. Therefore, the most significant aero-optical performance improvement was achieved at turret attitudes that do not align with the 'horn' vortices trajectory.

**Acknowledgments** This work has been supported by the Air Force Research Laboratory, Air Vehicle Directorate, WPAFB, OH and the Boeing Company. Support by the AFRL program manager Donnie Saunders and SARL-tunnel personnel is greatly appreciated.

## References

Andino MY, Wallace RD, Glauser MN, Camphouse RC, Schmit RF, Myatt JH (2011) Boundary feedback flow control: proportional control with potential application to aero-optics. AIAA J 49(1):32–40

Catrakis HJ, Apelian T, Goushcha O, Puga A, Hartwig D (2011) Active control of flow separation on a hemisphere with plasma forcing, AIAA Paper 2011–3991

Fitzgerald EJ, Jumper EJ (2004) The optical distortion mechanism in a nearly incompressible free shear layer. J.Fluid Mech 512:153–189

Gilbert J, Otten LJ (eds) (1982) Aero-Optical Phenomena, Progress in Astronautics and Aeronautics, vol 80. AIAA, New York

Gordeyev S, Jumper EJ (2010) Fluid dynamics and aero-optics of turrets. Prog Aerosp Sci 46:388–400

Gordeyev S, Post ML, MacLaughlin T, Ceniceros J, Jumper EJ (2007) Aero-optical environment around a conformal-window turret. AIAA J 45(7):1514–1524

Gordeyev S, Cress JA, Smith A, Jumper EJ (2010) Improvement in optical environment over turrets with flat window using passive flow control, AIAA Paper 2010–4492

Gregory JW, Sullivan JP, Raman G, Raghu S (2007) Characterization of the microfluidic oscillator. AIAA J 45:568–576

Jumper EJ, Fitzgerald EJ (2001) Recent advances in aero-optics. Prog Aerosp Sci 37:299–339

Morgan P, Visbal M (2009) Numerical simulations investigating control of flow over a turret, AIAA Paper 2009–2574

Palaviccini MR, George B, Cattafesta L (2011) Passive flow control over a three-dimensional turret with a flat aperture, AIAA Paper 2011–3265

Patil SKR, Ng TT (2010) Compressible wake stabilization using periodic porosity, AIAA Paper 2010–4834

Purohit SC, Shang JS, Hankey WL (1983) Effect of suction on the wake structure of a three-dimensional turret, AIAA Paper 83–1738

Schonberger JR, Fuhs AE, Mandigo AM (1982) Flow control for an airborne laser turret. J Aircraft 19(7):531–537

Tatarskii VI, Zavorotnyi VU (1985) Wave propagation in random media with fluctuating turbulent parameters. J Opt Soc Am A 2(12):2069–2076

Vukasinovic B, Glezer A (2007) Control of a separating flow over a turret, AIAA Paper 2007–4506

Vukasinovic B, Brzozowski D, Glezer A (2009) Fluidic control of separation over a hemispherical turret. AIAA J 47(9):2212–2222

Vukasinovic B, Glezer A, Gordeyev S, Jumper E, Kibens V (2010a) Fluidic control of a turret wake: aerodynamic and aero-optical effects. AIAA J 48(8):1686–1699

Vukasinovic B, Glezer A, Rusak Z (2010b) Dissipative small-scale actuation of a turbulent shear layer. J Fluid Mech 656:51–81

Vukasinovic B, Glezer A, Gordeyev S, Jumper E, Kibens V (2011) Hybrid control of a turret wake. AIAA J 49(6):1240–1255

Wallace RD, Shea PR, Glauser MN, Vaithianathan T, Carlson HA (2010) Feedback Flow Control for a Pitching Turret (Part II), AIAA Paper 2010–2361

Wallace RD, Shea PR, Glauser MN, Vaithianathan T, Carlson HA, Schmit R (2011) Suction flow control at high Reynolds number, AIAA Paper 2011–3716

Wang M, Mani A, Gordeyev S (2012) Physics and computation of aero-optics. Annu Rev Fluid Mech 44:299–321

Woszidlo R, Taubert L, Wygnanski I (2009) Manipulating the flow over spherical protuberances in a turbulent boundary layer. AIAA J 47(2):437–450